
Article:
Nott, JP, Pervolaraki, E, Benson, AP orcid.org/0000-0003-4679-9842 et al. (4 more authors) (2018) Diffusion Tensor Imaging determines three-dimensional architecture of human cervix: a cross sectional study. BJOG: An International Journal of Obstetrics & Gynaecology, 125 (7). pp. 812-818. ISSN 1470-0328

https://doi.org/10.1111/1471-0528.15002

Diffusion Tensor Imaging determines three-dimensional architecture of human cervix: a cross sectional study

James P. NOTT[1], Eleftheria PERVOLARAKI[3], Al P. BENSON[3,4], Elizabeth A. BONNEY[5], James D. PICKERING[2], Nafisa WILKINSON[5] and Nigel A.B. SIMPSON[1]

[1]Division of Women's and Children's Health and [2]Division of Anatomy, School of Medicine, [3]School of Biomedical Sciences and [4]Multidisciplinary Cardiovascular Research Centre, University of Leeds, [5]Leeds Teaching Hospitals NHS Trust, Leeds, UK

Correspondence: Mr. Nigel Simpson, Division of Women's and Children's Health, Level 9, Worsley Building, School of Medicine, University of Leeds, Clarendon Way, Leeds, LS2 9NL. E-mail: n.a.b.simpson@leeds.ac.uk Phone: 0113 393 3901

Running title: The three-dimensional structure of the human cervix

Abstract

Objective To determine the microarchitecture of the cervix using high resolution diffusion-tensor (DT) magnetic resonance imaging (MRI).

Design Cross-sectional study.

Setting Leeds, United Kingdom.

Population or Sample Women undergoing hysterectomy for benign pathology.

Methods Ex-vivo DT-MRI measurements were obtained using a 9.4T Bruker NMR on seven fixed human cervices obtained at hysterectomy. A deterministic fibre tracking algorithm was used to indirectly visualise underlying fibre organisation. Interregional differences in tissue structure were sought using quantitative measurements of diffusion.

Main outcome measures Identification of an occlusive structure in the region corresponding to the internal cervical os**.**

Results Fibre tracking demonstrated two regions: an outer circular and inner longitudinal layer. The total circumferential tract volume (TV) was greatest in the proximal region of the cervix (TV: proximal= 271 ± 198 mm^3, middle= 186 ± 119 mm^3, distal= 38 ± 36 mm^3). Fractional anisotropy (FA) and apparent diffusion coefficient(ADC) measurements were significantly different between regions in all

samples ($P < 0.0005$), indicating greater tract density and organisation towards the internal os.

Conclusions Fibre tracking infers a system of dense, well-defined, encircling fibres in the proximal region of the cervix, corresponding to the location of the internal os. These findings may provide evidence of specific anatomic microarchitecture within the cervix able to resist intrauterine forces associated with pregnancy.

Funding: The study was supported by a programme grant provided by Cerebra (grant identifier: RG.OBGY.485799; registered charity No: 1089812).

Keywords Cervix, internal os, pregnancy, preterm birth, cervical weakness, diffusion-tensor imaging

Tweetable abstract Diffusion-tensor MRI derived tractography identified well-defined encircling fibres at the internal os

Introduction

The human uterine cervix, a fibromuscular structure situated at the distal pole of the uterus, acts as a mechanical barrier and is key to the maintenance of pregnancy. This is largely achieved by its strength and length, preventing ascent of vaginal microorganisms into the uterine cavity and discouraging descent of the fetal membranes into the vagina.

During normal pregnancy the cervix is a load-bearing organ, resisting forces generated by the myometrium, fetus and amniotic sac.[1,2] Cervical change in response to intrauterine pressure typically presents within the midtrimester with funnelling of the internal os as seen on transvaginal ultrasound. Ultrasonography is therefore a tool to identify women who may be at risk of delivering early, as a short cervix is related to an increased risk of preterm birth, yet it fails to explain why cervical change presents in this way.[3]

A dense collagen network is thought to be central to resisting gestational forces and accounts for up to 80% of the subepithelial stroma.[4–7] By comparison, smooth muscle cells (18%) and elastin (<2%) form a small proportion,[4–6,8,9] though a progressive increase of smooth muscle is seen towards the internal os.[8,9] The respective roles and interplay between these stromal constituents remain largely unknown.

The biomechanical properties of the cervix are probably determined by the underlying fibre organisation and their directionality within the cervical stroma.[10,11] Imaging studies have sought to determine cervical fibre directionality using X-ray diffraction,[10] optical

coherence tomography,[11] second harmonic generation,[12] and diffusion tensor (DT) magnetic resonance imaging (MRI).[13,14] The results produced are varied, yet together suggest a circumferential band of fibres that encircle the cervical canal. It has since been postulated that this band of circular fibres probably resist the forces associated with cervical dilation.[15]

Given it is the internal os which typically funnels in cases of early cervical dilation, few studies have sought to describe the band of circular fibres in this region and whether differences exist when compared to distal regions of the cervix. Here we used DT-MRI and associated fibre tracking methods to further characterise the cervical structure.[16] This study also aimed to determine whether regional differences existed with regards to tissue properties as indicated by quantitative measurements of diffusion, tract orientation and volume.

Materials and Methods

Ethical approval was granted by the Yorkshire and Humber Regional Ethical Committee (reference number 15/YH/0111). Non-pregnant, premenopausal women undergoing total abdominal hysterectomy or vaginal hysterectomy for benign pathology were consented. No participants had a history of preterm birth, cervical weakness, or cervical excisional surgery.

Tissue preparation

Following hysterectomy, each uterus was immersed in a formal-saline solution (10% formalin, 0.9% sodium chloride, 4% formaldehyde) for 24 hours. The lower uterine pole and cervix were amputated from the remaining corpus via a transverse incision. The lower uterine pole and cervix were hemisected in the midsagittal plane and the right hemisection was made available for research. The lower uterine pole was subsequently detached from the cervix at the uterocervical junction. Each research sample was stored in a formal-saline solution for one week.

Prior to scanning, cervix samples were placed into polytetrafluorethylene (PTFE) cylindrical tube (Cole-Palmer, Illinois, USA) and immersed in Fomblin (Sigma-Aldrich, Missouri, USA).

Image acquisition

Diffusion images were acquired on a Bruker Biospin (Ettlingen, Germany) 9.4 T vertical NMR/S scanner with a 22 mm diameter imaging coil. A three-dimensional (3D) diffusion-weighted spin-echo sequence was applied at 20°C with the following parameters: echo-time (TE) = 15-60 ms, repetition time (TR) = 500-1000 ms, b = 1148 s/mm^2, averages 3-8, a matrix size = 256 × 256 × 256, slice thickness = 0.2 – 0.25 mm and an in-plane resolution = 0.2 – 0.25 mm. In each scan diffusion-weighted images were obtained in six directions, with an average scan time of 55 hours 24 minutes. The protocol has been described in detail previously, with the parameters modified for the current study.[17]

Image analysis and quantitative measurements

All data were analysed in DSI Studio (http://dsi-studio.labsolver.org).[16] Diffusion-tensor MRI yields quantitative values that infer tissue architecture by measuring the intrinsic properties of the diffusion of water. Fractional anisotropy (FA) quantifies the deviation from isotropic diffusion on a continuum from 0 (isotropic/equal in all directions) to 1 (anisotropic/directionally dependent).[18] FA was calculated as follows:

$$FA = \sqrt{\frac{3}{2} \cdot \frac{(\lambda_1 - \langle\lambda\rangle)^2 + (\lambda_2 - \langle\lambda\rangle)^2 + (\lambda_3 - \langle\lambda\rangle)^2}{{\lambda_1}^2 + {\lambda_2}^2 + {\lambda_3}^2}}$$

$$\langle\lambda\rangle = \frac{\lambda_1 + \lambda_2 + \lambda_3}{3}$$

where λ_1, λ_2, λ_3 correspond to the primary, secondary and tertiary eigenvalues of the diffusion tensor, respectively.[17] The magnitude of diffusion, expressed as the apparent diffusion coefficient (ADC), is a measurement that reflects tract density and was calculated as follows:

$$S(b) = S(0) * \exp(-b * ADC)$$

where S(0) and S(b) are the signal intensities of each voxel obtained with the b-values 0 and 1148 s/mm^2 respectively.[19] Larger ADC values correspond to decreased tract density. In this study, each image of the cervix was divided into five portions with respect to the length of each sample and the upper (proximal), middle and lower (distal) portions were selected for analysis. Regional FA and ADC intra-sample differences were determined for proximal, middle and distal transverse regions of interest (ROI).

Fibre tracking methods

A deterministic fibre tracking algorithm was applied to identify, visualise, and quantify the tracts within each cervix.[16] Fibres were visualised if FA was greater than 0.2, if the principal diffusion direction diverged by less than 35° compared to that of the previous voxel, and if the length of the fibre was greater than 10 mm. Transverse ROI were segmented at the proximal, middle and distal regions of each cervix. Circumferential tracts were depicted in these regions by segmenting each ROI in the mid-sagittal plane; tracts were visualised if they passed through the ROI. Total tract volume (mm^3) was calculated in DSI Studio for each of the three regions.

Statistics

Kruskal-Wallis rank sum tests were conducted to determine intra-sample differences in FA and ADC, and Eta squared (η^2) was used to calculate effect size. The output of η^2 indicated the percentage variance in the dependent variable that was explained by the independent variable. Subsequent pairwise comparisons were performed using Dunn's procedure.[20] A Welch ANOVA was conducted to determine inter-sample differences in tract volume in the segmented regions of the cervix. Subsequent pairwise comparisons were made using Games-Howell post hoc analysis.

Data were presented as mean ± standard deviation with a statistical significance accepted at $p < 0.05$. All statistical analyses were performed using SPSS software v.23.0 (SPSS, Inc., Chicago, IL).

Results

Seven patients were consented and cervical tissue was collected. Of these women, six were multiparous and one was nulliparous. The mean age of the patients was 44 years (Table 1).

Qualitative findings

Analysis of colour-coded vector maps demonstrated a microarchitecture common to each cervix sample. In slices orthogonal to the long axis, an inner longitudinal layer and an outer circular layer were consistently identified at the proximal and middle portions of the cervix (Fig. 1A and B), though both were less evident towards the distal cervix (Fig. 1C and D).

The randomised fibre tracking reconstruction of approximately 5,000 fibres further confirmed inner longitudinal tracts extending from the proximal to the middle cervix parallel to the cervical canal, and outer encircling tracts (Fig. 2A and E; Video S1). Segmentation of the encircling tracts in the proximal, middle and distal cervix showed that this system of fibres became more prominent towards the proximal cervix (proximal = 271 ± 198 mm^3, middle = 186 ± 119 mm^3, distal = 38 ± 36 mm^3; Fig. 2 and Fig. S1). Measurements in the three regions were found to be significantly different (Welch's $F(2, 8.896) = 8.536$, $p < 0.009$). Post hoc analysis demonstrated a significant increase in tract volume (mm^3) from the distal to middle regions (147.8 mm^3, 95% CI 9.8 to 285.8,

p = 0.038) and from distal to proximal regions (233.2 mm^3, 95% CI 4.0 to 462.3, p = 0.047).

Quantitative evaluation

Intra-sample comparisons of FA demonstrated that regional measurements were significantly different ($p < 0.0005$) following Kruskal-Wallis analysis (Table S1; Fig. S2). The proportion of variability in FA accounted for by region ranged from 4% – 29%. In all instances, pairwise comparisons demonstrated significant differences ($p < 0.0005$) between regions. Mean FA values were largest in the proximal region in all samples and values progressively decreased towards the distal region in six samples, indicating that tract organisation increased towards the proximal cervix. Similarly, Kruskal-Wallis analysis demonstrated ADC measurements were significantly different between regions ($p < 0.0005$), with the proportion of variability in ADC accounted for by region ranging 4% - 30% (Table S2; Fig. S3). Pairwise comparisons demonstrated significant differences ($p < 0.0005$) between all regions. Measurements of ADC were found to be lower in the proximal portion and progressively increased towards the distal region in six of the samples, indicating that tract density increased towards the proximal cervix. In the remaining sample, the ADC value was lowest in the middle region, followed by the proximal and distal regions.

Discussion

Main findings

DT-MRI and fibre tracking indicated a region of encircling fibres in the proximal region of the cervix, a location which corresponds to the internal os. Quantitative measurements of diffusion have also demonstrated greater tract uniformity and density in this region.

Strengths and limitations of the study

This study used a high-resolution 3D imaging technique that allowed for analysis along the length of the cervix, which in turn allowed for the determination of regional differences in tissue properties as measured by quantitative measurements of diffusion.

There were several limitations associated with the study. Firstly, the data were obtained from a small sample of women that had already received conservative management and then a subsequent hysterectomy for benign gynaecologic pathology, and therefore may not be representative of a larger population of healthy women. For example, it is possible that treatment with gonadotropin-releasing hormone (GnRH) analogues may influence fibre density and thereby MR imaging. Secondly, ex-vivo imaging of fixed samples may be considered artificial and not comparable to in-vivo DT-MRI measurements. However, imaging of fixed tissues provides the opportunity for longer scan times and images of greater resolution.[21] A general consensus must still be reached on whether tissue fixation alters the quantitative measurements that are yielded by diffusion imaging, yet regional differences observed in in-vivo and fresh tissue imaging are observed in formalin fixed samples.[22,23] Further, comparisons with fresh tissue imaging show that although tissue shrinkage is observed following fixation, no obvious changes are seen in the orientation of the primary eigenvector.[23]

Consequently, ex-vivo DT-MRI is becoming common place in laboratory imaging studies.

Interpretation

The inference of encircling fibres within the cervix correlates well with previous ultrastructural studies.[10,11] Furthermore, the two distinct fibre zones seen were in accord with previous ex-vivo and in-vivo DT-MRI observations.[13,14] The prominence of the encircling fibres at the internal os may provide evidence of a specific microarchitecture that resists forces associated with pregnancy and encourages the possibility of an occlusive structure corresponding to this region of the cervix. Such an observation is consistent with previous biomechanical modelling.[1] How this translates to the clinical setting requires further study and inquiry. Nonetheless, it could be inferred that mid-trimester funnelling of the internal os, as observed on ultrasound, may be due to an absence of or damage to these prominent encircling fibres.

Further investigation should also consider the composition of these encircling fibres at the internal os. The prevailing description of cervical morphology would suggest that these fibres are collagenous in nature, as it was previously noted that cervical stroma contains a minimal cellular component.[4–6,24] Recently, however, new insights were offered following improved immunohistochemical analysis of two-dimensional sections and functional studies.[9] Cervical smooth muscle cells were found to be circumferentially orientated around the periphery of the cervix and were most abundant at the internal os. Further, cervical tissue was seen to contract in response to oxytocin, with the internal os contracting with more force than the external os. Future studies could

consider three-dimensional reconstructive modelling of digitised histologic sections, to provide further insight into the occlusive structure at the internal os.

Quantitative measurements of diffusion demonstrate that the cervix is not a uniform structure, supporting previous histologic and radiographic observations.[8,25,26] Significant differences were observed in each identified region with regards to measurements of FA and ADC. However, this should be interpreted with caution, as the effect size ranged from weak to fairly strong across the sample for both quantitative measurements and therefore significance may have been achieved due to the volume of data being studied. Nonetheless, findings indicate that tract uniformity and density differ throughout the cervix at an intravoxel level, as 86% of the observations in the present study demonstrated that tract uniformity and density progressively increase towards the internal os. These regional differences may be reflected in the mechanical strength and performance of each region, though further investigation is necessary for this to be confirmed. In clinical practice digital examination of the cervix during pregnancy sometimes shows a dilated external os whilst the internal os remains closed, which could be explained by the structural differences seen in this study.[27]

The in-vivo application of DT-MRI to indirectly discern the fibre architecture of the human cervix may serve as biomarker to identify those who may have a weak cervix. This application is contingent on the trade-off between spatial resolution, scan time and signal-to-noise ratio. With advances in DT-MRI schemes, imaging at a sub-millimetre scale in-vivo using a 3T clinical scanner may be achievable.[28] However, the feasibility and acceptability of high-resolution DT-MRI use in the clinical setting, while technically possible, is yet to ascertained. Future research may consider using such

novel DT-MRI schemes to determine whether detailed images of the cervix can be obtained in this manner, but this was not within the scope of this study.

Conclusion

DT-MRI has been seen to be an effective tool in providing high resolution images of the human cervix. Quantitative evaluation demonstrated increased tract uniformity and density within the cervix towards the proximal region. Fibre-tracking provided evidence of a system of dense, well-defined, encircling fibres corresponding to the location of the internal os. These observations encourage the re-examination of the role of the internal os during pregnancy and prompt the development of high resolution clinical imaging to examine this region in clinical practice.

Acknowledgements

We wish to acknowledge the women who kindly gave consent to participate in the research and the members of staff in the histopathology department at the Leeds Teaching Hospitals Trust.

Disclosure of interests

Nothing to disclose

Contribution to Authorship

JN was responsible for study design, data collection, data collation and analysis, and was the author of the manuscript. EP and AB were responsible for study design, data collection, and reviewed and edited the manuscript. NW was responsible for data collection and reviewed and edited the manuscript. NS, JP and EB were responsible for study design and reviewed and edited the manuscript.

Details of Ethics Approval

Ethics approval was granted by the Yorkshire and Humber Regional Ethical Committee (reference number: 15/YH/0111; date: 14/5/15).

Funding

The study was supported by a programme grant provided by Cerebra (grant identifier: RG.OBGY.485799; registered charity No: 1089812).

References

1. House M, McCabe R, Socrate S. Using imaging-based, three-dimensional models of the cervix and uterus for studies of cervical changes during pregnancy. Clin Anat. 2013;26(1):97–104.
2. Myers KM, Feltovich H, Mazza E, Vink J, Bajka M, Wapner RJ, et al. The mechanical role of the cervix in pregnancy. J Biomech. 2015;48(9):1511–23.
3. Iams J, Goldenberg R. The length of the cervix and the risk of spontaneous premature delivery. New Engl Jounal Med. 1996;334(9):567–72.
4. Danforth DN. The Fibrous Nature of the Human Cervix, and its relation to the

isthmic segment in gravid and nongravid uteri. Am J Obstet Gynecol. 1947;53(4):541–60.

5. Danforth DN. The distribution and functional activity of the cervical musculature. Am J Obstet Gynecol. 1954;68(5):1261–71.

6. Hughesdon PE. The fibromuscular structure of the cervix and its changes during pregnancy and labour. BJOG An Int J Obstet Gynaecol. 1952;59(6):763–76.

7. Uldbjerg N, Ekman G, Malmström A, Olsson K, Ulmsten U, Forman A, et al. Ripening of the human uterine cervix related to changes in collagen, glycosaminoglycans, and collagenolytic activity. Am J Obstet Gynecol. 1983 Nov;147(6):662–6.

8. Rorie DK, Newton M. Histologic and chemical studies of the smooth muscle in the human cervix and uterus. Am J Obstet Gynecol. 1967;99(4):466–9.

9. Vink JY, Qin S, Brock CO, Zork NM, Feltovich HM, Chen X, et al. A new paradigm for the role of smooth muscle cells in the human cervix. Am J Obstet Gynecol. 2016; 215(4):478.

10. Aspden RM. Collagen Organisation in the Cervix and its Relation to Mechanical Function. Coll Relat Res. 1988;8(2):103–12.

11. Gan Y, Yao W, Myers KM, Vink JY, Wapner RJ, Hendon CP. Analyzing three-dimensional ultrastructure of human cervical tissue using optical coherence tomography. Biomed Opt Express. 2015;6(4):1090–108.

12. Reusch LM, Feltovich H, Carlson LC, Hall G, Campagnola PJ, Eliceiri KW, et al. Nonlinear optical microscopy and ultrasound imaging of human cervical structure. J Biomed Opt. 2013;18(3):31110.

13. Weiss S, Jaermann T, Schmid P, Staempfli P, Boesiger P, Niederer P, et al. Three-dimensional fiber architecture of the nonpregnant human uterus determined

ex vivo using magnetic resonance diffusion tensor imaging. Anat Rec A Discov Mol Cell Evol Biol. 2006;288(1):84–90.

14. Fujimoto K, Kido A, Okada T, Uchikoshi M, Togashi K. Diffusion tensor imaging (DTI) of the normal human uterus in vivo at 3 tesla: comparison of DTI parameters in the different uterine layers. J Magn Reson Imaging. 2013;38(6):1494–500.

15. Myers KM, Hendon CP, Gan Y, Yao W, Yoshida K, Fernandez M, et al. A continuous fiber distribution material model for human cervical tissue. J Biomech. 2015;48(9):1533–40.

16. Yeh F-C, Verstynen TD, Wang Y, Fernández-Miranda JC, Tseng W-YI. Deterministic diffusion fiber tracking improved by quantitative anisotropy. PLoS One. 2013;8(11):e80713.

17. Pervolaraki E, Anderson RA, Benson AP, Hayes-Gill B, Holden A V, Moore BJR, et al. Antenatal architecture and activity of the human heart. Interface Focus. 2013;3(2):20120065.

18. Pfefferbaum A, Sullivan E V, Hedehus M, Lim KO, Adalsteinsson E, Moseley M. Age-related decline in brain white matter anisotropy measured with spatially corrected echo-planar diffusion tensor imaging. Magn Reson Med. 2000;44(2):259–68.

19. Pervolaraki E, Dachtler J, Anderson RA, Holden A V. Ventricular myocardium development and the role of connexins in the human fetal heart. Sci Reports. 2017;7(1):12272.

20. Dunn O. Multiple comparisons using rank sums. Technometrics. 1964;6:241–52.

21. Guilfoyle DN, Helpern JA, Lim KO. Diffusion tensor imaging in fixed brain

tissue at 7.0 T. NMR Biomed. 2003;16(2):77–81

22. Sun S-W, Neil JJ, Song S-K. Relative indices of water diffusion anisotropy are equivalent in live and formalin-fixed mouse brains. Magn Reson Med. 2003;50(4):743–8.

23. Bourne RM, Bongers A, Chatterjee A, Sved P, Watson G. Diffusion anisotropy in fresh and fixed prostate tissue ex vivo. Magn Reson Med. 2016;76(2):626–34.

24. Oxlund BS, Ørtoft G, Brüel A, Danielsen CC, Bor P, Oxlund H, et al. Collagen concentration and biomechanical properties of samples from the lower uterine cervix in relation to age and parity in non-pregnant women. Reprod Biol Endocrinol. 2010;8:82.

25. Leppert P, Cerreta J, Mandl I. Orientation of elastic fibers in the human cervix. Am J Obstet Gynecol. 1986;155(1):219–24

26. DeSouza NM, Hawley IC, Schwieso JE, Gilderdale DJ, Soutter WP. The uterine cervix on in vitro and in vivo MR images: a study of zonal anatomy and vascularity using an enveloping cervical coil. AJR Am J Roentgenol. 1994;163(3):607–12.

27. Zork NM, Myers KM, Yoshida K, Cremers S, Jiang H, Ananth C V, et al. A systematic evaluation of collagen cross-links in the human cervix. Am J Obstet Gynecol. 2015;212(3):321.e1-8.

28. Chang H-C, Sundman M, Petit L, Guhaniyogi S, Chu M-L, Petty C, et al. Human brain diffusion tensor imaging at submillimeter isotropic resolution on a 3Tesla clinical MRI scanner. Neuroimage. 2015;118:667–75.

Table 1. Patient demographics for cervical samples

Patient no.	Age (years)	Parity	Obstetric History	Diagnosis	Pre-hysterectomy interventions
1	49	3	3 x NVD	Fibroid uterus	Hysteroscopy GnRH analogue Progestin
2	43	1	1 x CD	Fibroid uterus	GnRH analogue
3	46	3	3 X NVD	Stage III cystocele Stage III uterocervical decent	Progestin Physiotherapy management
4	42	2	2 x NVD	Endometriosis Fibroid uterus	Hysteroscopy Endometrial ablation GnRH analogue
5	47	2	2 X NVD	Uterine prolapse	Physiotherapy management
6	36	0	N/A	Endometriosis	GnRH analogue
7	45	3	3 x NVD	Fibroid uterus	Tranexamic acid

NVD- Normal vaginal delivery

CD- Caesarian delivery

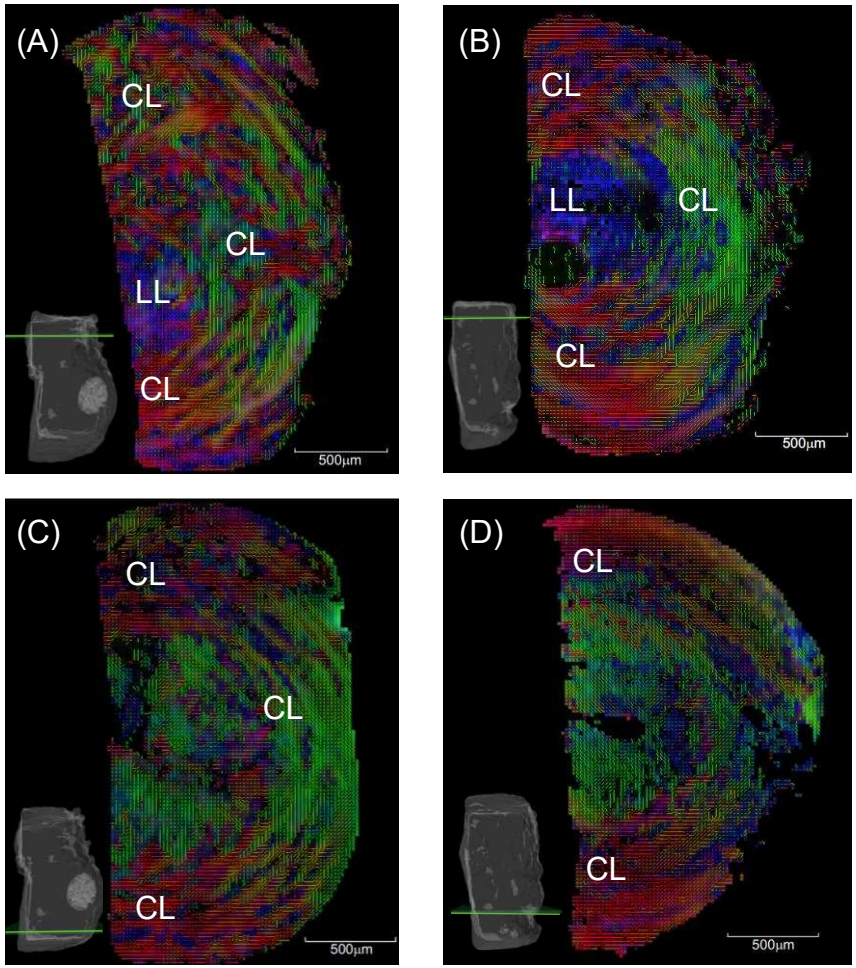

Figure 1. Colour vector maps depicting principal diffusion directions on slices orthogonal to the long axis at proximal (A, B,) and corresponding distal (D, E,) regions. Colours reflect the orientation of the principal diffusion vector with respect to Cartesian axes system (x=red, y=green, z=blue). Slice positions are indicated in bottom corners by the green cut plane. A longitudinal layer (LL) and circular layer (CL) are identifiable in proximal region of both samples (A, B). The outer circular layer extends towards the distal region in both samples, yet the longitudinal layer less evident in the distal region (C, D).

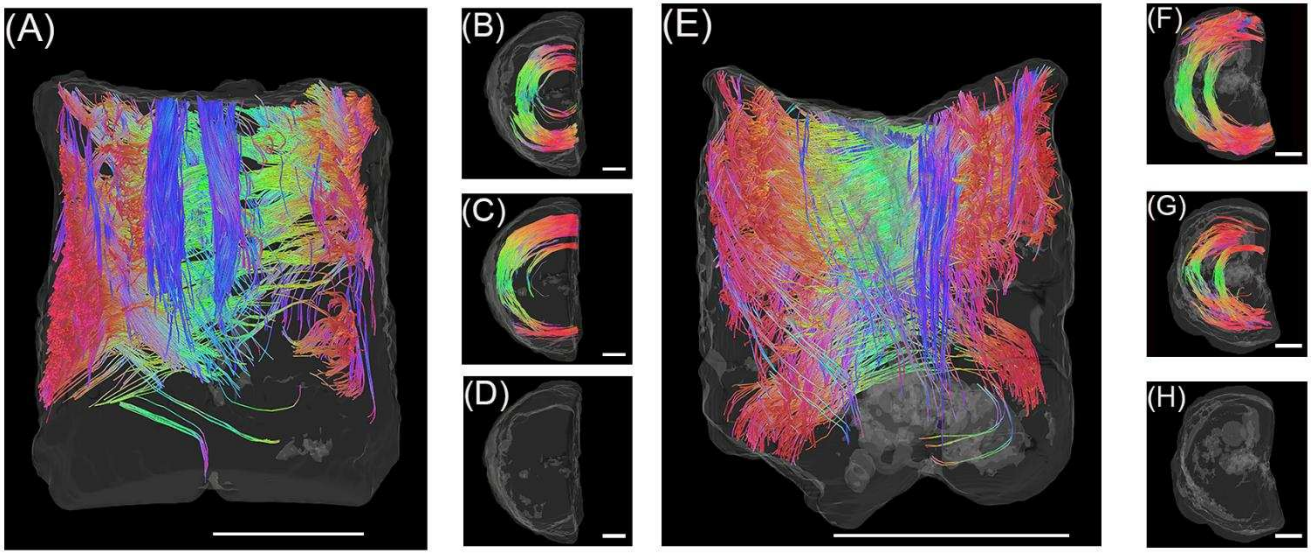

Figure 2. 3D tractography computed using a deterministic fibre-tracking algorithm. The surface of the cervix is indicated by the grey scale border. Colours reflect orientation of fibres (x=red, y=green, z=blue). A, E: Images display midline surfaces of hemisected samples four (A) and five (E). Both samples demonstrate two ROIs: inner longitudinal (blue) and outer circumferential (red, green). Corresponding transverse cross-sections depict encircling fibres at the respective proximal (B, F) middle (C, G) and distal (D, H) regions of each sample (scale bar = 500μm).

Supporting Information

Table S1. Intra-sample comparisons of FA

Sample	Region	No. of Voxels	Mean (±SD)	X^2	η^2
1	Prox	151142	0.2766 (.0948)	86028.161	0.12
	Middle	226368	0.2102 (.0955)		
	Distal	189471	0.1784 (.07424)		
2	Prox	67639	0.2671 (.11818)	22615.848	0.13
	Middle	83792	0.1878 (.10132)		
	Distal	20986	0.2043 (.10392)		
3	Prox	263717	0.4761 (.17810)	83976.474	0.09
	Middle	409481	0.3830 (.16526)		
	Distal	216986	0.3360 (.14975)		
4	Prox	209250	0.2646 (.11391)	17818.661	0.02
	Midde	239032	0.2474 (.10357)		
	Distal	173430	0.2241 (.11190)		
5	Prox	315890	0.3876 (.15805)	150754.068	0.39
	Middle	426471	0.3087 (.14362)		
	Distal	185907	0.2122 (.13722)		
6	Prox	4670	0.3402 (.18635)	2303.936	0.002
	Middle	4878	0.2111 (.14779)		
	Distal	3410	0.1867 (.13333)		
7	Prox	4279	0.2039 (.09724)	2008.283	0.15
	Middle	5889	0.1547 (.08907)		
	Distal	4429	0.1237 (.04802)		

Table S2 Intra-sample comparisons of ADC

Sample	Region	Total no. of Voxels	Mean (±SD)*	X^2	η^2
1	Prox	566981	0.7742 (.11941)	50882.938	0.08
	Middle		0.8712 (.23155)		
	Distal		0.8800 (.15650)		
2	Prox	172420	0.7170 (.22392)	18528.390	0.11
	Middle		0.8142 (.22284)		
	Distal		0.8909 (.21032)		
3	Prox	890184	0.5585 (.19503)	93450.008	0.1
	Middle		0.5851 (.19933)		
	Distal		0.6985 (.19827)		
4	Prox	621712	0.7743 (.23289)	58766.115	0.09
	Middle		0.7517 (.19514)		
	Distal		0.8720 (.19818)		
5	Prox	928268	0.5712 (.18486)	195267.162	0.21
	Middle		0.6358 (.23909)		
	Distal		0.9192 (.33924)		
6	Prox	12958	0.8126 (.38046)	3557.017	0.27
	Middle		1.0655 (.38046)		
	Distal		1.4323 (.43714)		
7	Prox	14597	1.0148 (.23077)	4350.022	0.30
	Middle		1.2633 (.31466)		
	Distal		1.3766 (.20235)		

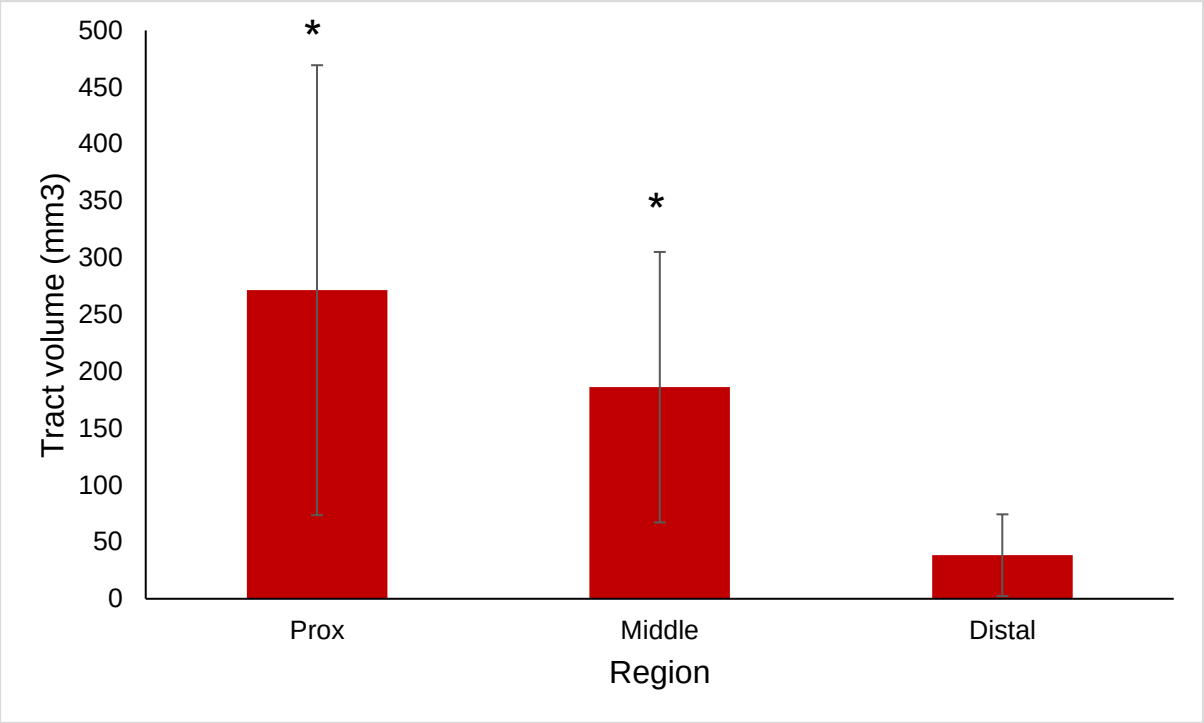

Figure S1 Volume of circumferential fibres increase towards the proximal region of the cervix. The values are expressed as mean ± SD (n = 7). * Indicates significant difference relative to distal region of cervix, $P < 0.05$ (Welch ANOVA).

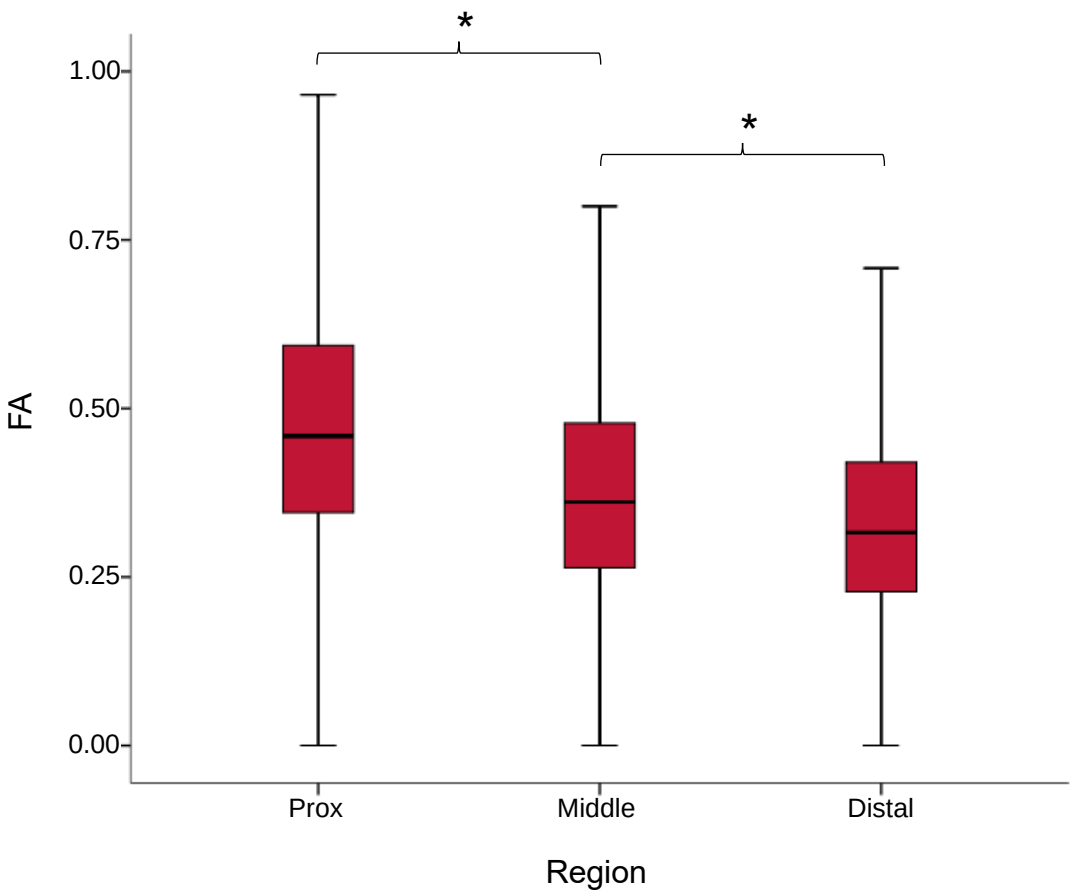

Figure S2. Regional FA values recorded in a representative sample. FA increases towards proximal region of cervix, indicating that tract alignment increases towards the internal os. The trend observed was observed in six samples. * $p<0.0005$

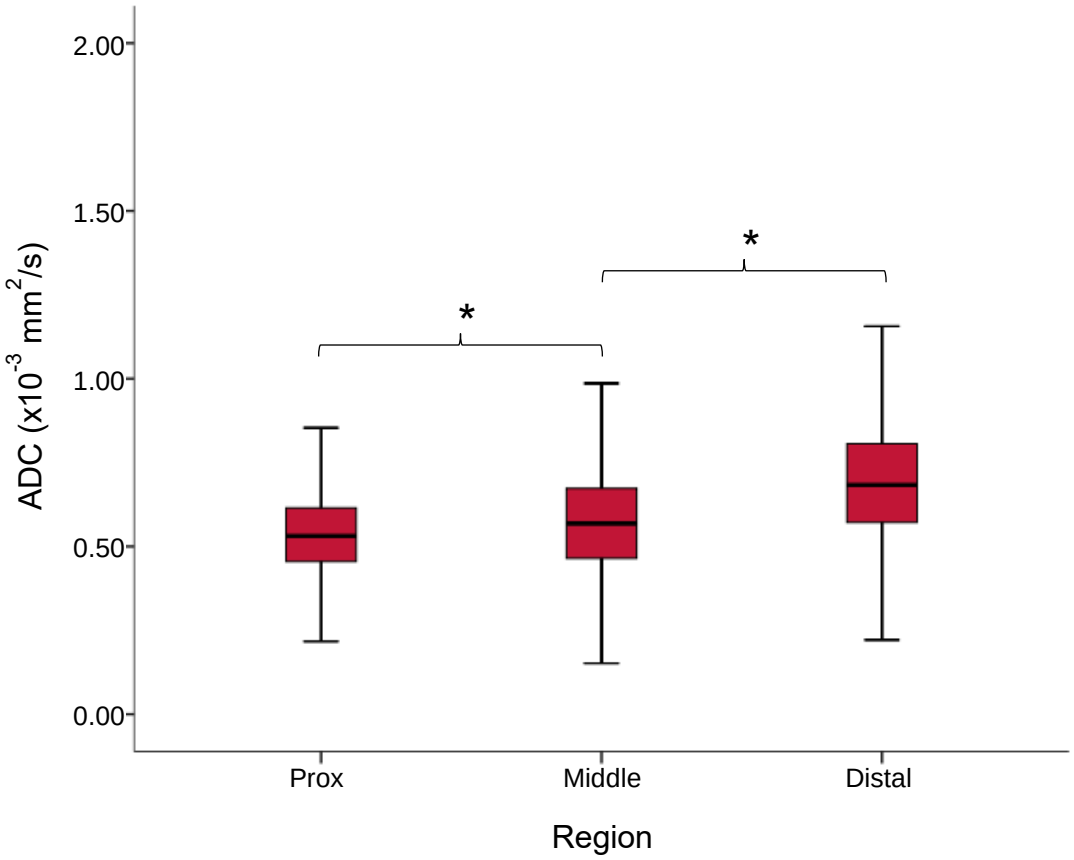

Figure S3. Regional ADC values recorded in a representative sample. ADC decreases towards proximal region of cervix, indicating that tract density increases towards the internal os. The trend observed was observed in six samples. * $p<0.0005$.